Available online at www.sciencedirect.com
SCIENCE DIRECT
International Journal of Heat and Fluid Flow 27 (2006) 436–444
International Journal of HEAT AND FLUID FLOW
www.elsevier.com/locate/ijhff

Drag reduction by gas injection into turbulent boundary layer: Density ratio effect

P.V. Skudarnov, C.X. Lin *

Applied Research Center, Florida International University, 10555 W. Flagler St., EC 2100, Miami, FL 33174, USA

Received 30 November 2004; received in revised form 21 November 2005
Available online 3 February 2006

Abstract

A two-dimensional single phase computational fluid dynamics (CFD) model of microbubble-laden flow over a flat plate was used to assess the role of mixture density variation in microbubble drag reduction. The model consisted of Reynolds-averaged Navier–Stokes (RANS) transport equations, a standard k–ω turbulence model, and a convection–diffusion species transport model. Performance of the model was validated with available experimental data and numerical simulations of more advanced multiphase two-fluid model. A parametric study of the density ratio effect on the drag reduction was carried out. The study indicated that simple mixture density variation effect plays one of the major roles in the microbubble drag reduction phenomenon. Also, the influence of the density ratio (the ratio of density of injected gas to that of water) on gas volume fraction profiles was found to be minimal within studied parameter range.

Keywords: Microbubble drag reduction; Flat plate

1. Introduction

The skin friction drag reduction has been a subject of extensive research during the past several decades. By reducing the skin friction drag an increased range or speed of the surface vessels, and underwater vehicles can be achieved. One of the methods to reduce the skin friction drag is gas injection into a liquid boundary layer, such injection results in the formation of microbubbles that produces drag reduction. This technique is called microbubble drag reduction (MDR) and is able to provide drag reductions of as much as 80%. MDR offers great potential in Naval applications.

McCormick and Bhattacharya (1973) reported the first microbubble drag reduction experiments. During the past decades, many research efforts have been devoted to microbubble drag reduction (Merkle and Deutsch, 1992). The work conducted by researchers in the former Soviet Union and in the United States, primarily by the Applied Research Laboratory (ARL) at The Pennsylvania State University, provided the benchmark in microbubble drag reduction research. It has been found that there are many factors that influence microbubble drag reduction, including air jet flow rate, injection process, free stream velocity, pore size, buoyancy, and surface configuration. As evidenced by published papers in the open literature, most of the previous studies of microbubble drag reduction were conducted experimentally. Due to the complexity of microbubble laden boundary layers, theoretical investigations have fallen behind the progress made by experimental studies. It is recognized that a better understanding of the microbubble drag reduction mechanism is critical to its optimal performance with minimal use of gas volume in practical applications.

In recent years, analytical computational modeling of microbubble drag reduction has been attempted by several researchers (Madavan et al., 1985; Marie, 1987; Kim and

* Corresponding author. Tel.: +1 305 348 1596; fax: +1 305 348 1852.
E-mail address: chengxian.lin@arc.fiu.edu (C.X. Lin).

0142-727X/$ - see front matter © 2005 Elsevier Inc. All rights reserved.
doi:10.1016/j.ijheatfluidflow.2005.12.002

Nomenclature

A	area, m^2
C_f	integrated drag coefficient over "Wall 3" flat plate section, dimensionless
$DR = \frac{\rho_{gas}}{\rho_{water}}$	density ratio, dimensionless
p	pressure, Pa
Q	flow rate, m^3/s
Re	Reynolds number, dimensionless
t	time, s
U_∞	free-stream velocity, m/s
u_i	mean velocity components ($i = 1, 2, 3$), m/s
u_i'	fluctuating velocity components ($i = 1, 2, 3$), m/s
$u_\tau = \sqrt{\frac{\tau_w}{\rho}}$	friction velocity, m/s
$u^+ = \frac{u}{u_\tau}$	velocity in inner variables, dimensionless
y	wall normal coordinate, m
$y^+ = \frac{\rho u_\tau y}{\mu}$	wall normal coordinate in inner variables, dimensionless
μ	dynamic viscosity, Pa s
ρ	density, kg/m^3
τ_w	wall shear stress, Pa

Cleaver, 1995; Meng and Uhlman, 1998; Xu et al., 2002; Kunz et al., 2003) to reveal the mechanism of the microbubble drag reduction phenomenon. A study by Legner (1984) proposed a simple stress model for gas bubble drag reduction and indicated that the drag reduction was caused by a combination of density reduction and turbulence modification. Meng and Uhlman (1998) suggested that bubble splitting was a plausible basic mechanism for reducing turbulence in a microbubble-laden turbulent boundary layer. Another new development in microbubble drag reduction studies is application of Direct Numerical Simulation (DNS) to the problem of bubbly flows. Application of DNS to model microbubble drag reduction was recently undertaken by Kanai and Miyata (2001), Kawamura and Kodama (2002), and Ferrante and Elghobashi (2004). Kanai and Miyata (2001) explained the mechanism of drag reduction via prevention of spanwise vorticity formation near the wall due to the bubbles, which leads to suppression of turbulence bursting phenomenon and reduction of turbulent energy. Kawamura and Kodama (2002) did not obtain drag reduction in their simulation suggesting this to be due to the low Reynolds number and the large bubble size. Ferrante and Elghobashi (2004), on the other hand, obtained significant drag reduction for very small volume fraction of bubbles, which they attributed to reduced streamwise velocity in the wall streaks due to the presence of the bubbles. It should be pointed out that although DNS is powerful in elucidating physical mechanisms it is very computationally intensive. For this reason the above DNS modeling was done for low Reynolds number flows. None of the DNS modeling results was verified with experimental data because experiments were conducted at high Reynolds numbers typical for practical applications. While the outlined efforts made impressive progress toward the in-depth understanding of the mechanism from various angles, the available theoretical work is not sufficient to answer all the questions associated with microbubble drag reduction. The relative importance of postulated mechanisms remains unclear. It has been suggested (Legner, 1984 and Madavan et al., 1985) that a simple density effect is the dominant source of drag reduction.

In this paper the role of mixture density variation in microbubble drag reduction was assessed via simple single phase numerical model for the high Reynolds number microbubble-laden flow over a flat plate. Following sections give detailed description of the model and its validation, and present results of the parametric study of the density ratio effect on the drag reduction. The performed study indicates that simple mixture density variation effect plays one of the major roles in the microbubble drag reduction phenomenon.

2. Numerical model

To perform computational assessment of the role of mixture density variation in microbubble drag reduction, a two-dimensional computational fluid dynamics (CFD) model of microbubble-laden flow over a flat plate was developed. The model consisted of Reynolds-averaged Navier–Stokes (RANS) transport equations and a standard k–ω turbulence model (Wilcox, 1998) with a low Reynolds number correction. This model was designed to be applied throughout the boundary layer when the near wall mesh is sufficiently fine. The RANS transport equations are

$$\frac{\partial \rho}{\partial t} + \frac{\partial}{\partial x_i}(\rho u_i) = 0 \tag{1}$$

$$\frac{\partial}{\partial t}(\rho u_i) + \frac{\partial}{\partial x_j}(\rho u_i u_j) = -\frac{\partial p}{\partial x_i} + \frac{\partial}{\partial x_j}\left[\mu\left(\frac{\partial u_i}{\partial x_j} + \frac{\partial u_j}{\partial x_i} - \frac{2}{3}\delta_{ij}\frac{\partial u_l}{\partial x_l}\right)\right] + \frac{\partial}{\partial x_j}(-\rho\overline{u_i' u_j'}) \tag{2}$$

In the Eqs. (1) and (2) as well as subsequent equations ρ and μ are the mixture density and viscosity respectively, which are defined in (12) and (13) below. The last term in Eq. (2), called the Reynolds stresses, is related to mean velocity gradients using Boussinesq hypothesis:

$$-\rho\overline{u_i' u_j'} = \mu_t\left(\frac{\partial u_i}{\partial x_j} + \frac{\partial u_j}{\partial x_i}\right) - \frac{2}{3}\left(\rho k + \mu_t \frac{\partial u_i}{\partial x_i}\right)\delta_{ij} \tag{3}$$

The transport equations for the turbulence kinetic energy k and the specific dissipation rate ω are

$$\frac{\partial}{\partial t}(\rho k)+\frac{\partial}{\partial x_i}(\rho k u_i)=\frac{\partial}{\partial x_j}\left(\Gamma_k\frac{\partial k}{\partial x_j}\right)+G_k-Y_k \tag{4}$$

$$\frac{\partial}{\partial t}(\rho \omega)+\frac{\partial}{\partial x_i}(\rho \omega u_i)=\frac{\partial}{\partial x_j}\left(\Gamma_\omega\frac{\partial \omega}{\partial x_j}\right)+G_\omega-Y_\omega \tag{5}$$

where Γ_k and Γ_ω are the effective diffusivity of k and ω, respectively; $G_k=\mu_t 2S_{ij}S_{ij}$ $\left(\text{where } S_{ij}=\frac{1}{2}\left(\frac{\partial u_j}{\partial x_i}+\frac{\partial u_i}{\partial x_j}\right)\right)$ is the generation of turbulence kinetic energy due to mean velocity gradients; $G_\omega=\alpha\frac{\omega}{k}G_k$ is the generation of ω; and $Y_k=\rho\beta^* f_{\beta^*}k\omega$ and $Y_\omega=\rho\beta f_\beta\omega^2$ are the dissipation of k and ω due to turbulence.

The low Reynolds number correction is achieved by introducing damp coefficient α^* into the turbulent viscosity equation as shown below (Wilcox, 1998)

$$\mu_t=\alpha^*\frac{\rho k}{\omega} \tag{6}$$

$$\alpha^*=\alpha^*_\infty\left(\frac{\alpha^*_0+Re_t/R_k}{1+Re_t/R_k}\right) \tag{7}$$

where $\alpha^*_\infty=1$; $Re_t=\frac{\rho k}{\mu\omega}$; $R_k=6$; $\alpha^*_0=\frac{\beta_i}{3}$; $\beta_i=0.072$. The rest of the coefficients used in the above equations are defined as follows (Wilcox, 1998):

$$\alpha=\frac{\alpha_\infty}{\alpha^*}\left(\frac{\alpha_0+Re_t/R_\omega}{1+Re_t/R_\omega}\right),\quad \alpha_\infty=0.52,\quad R_\omega=2.95$$

$$\beta^*=\beta^*_\infty\left(\frac{4/15+(Re_t/R_\beta)^4}{1+(Re_t/R_\beta)^4}\right),\quad R_\beta=8,\quad \beta^*_\infty=0.09$$

$$f_{\beta^*}=\begin{cases}1 & \chi_k\leqslant 0\\ \frac{1+680\chi_k^2}{1+400\chi_k^2} & \chi_k\geqslant 0\end{cases},\quad \chi_k=\frac{1}{\omega^3}\frac{\partial k}{\partial x_j}\frac{\partial \omega}{\partial x_j}$$

$$\beta=0.072,\quad f_\beta=\frac{1+70\chi_\omega}{1+80\chi_\omega},$$

$$\chi_\omega=\left|\frac{\Omega_{ij}\Omega_{jk}S_{ki}}{(\beta^*_\infty\omega)^3}\right|,\quad \Omega_{ij}=\frac{1}{2}\left(\frac{\partial u_i}{\partial x_j}-\frac{\partial u_j}{\partial x_i}\right)$$

Wall boundary condition for the turbulence kinetic energy is

$$\frac{\partial k}{\partial n}=0 \tag{8}$$

where n is the local coordinate normal to the wall.

Wall boundary condition for the specific dissipation rate is

$$\omega_w=\frac{\rho u_\tau^2}{\mu}\omega^+,\quad \text{where } \omega^+=\min\left(2500,\frac{6}{0.09\cdot(y^+)^2}\right) \tag{9}$$

Mixture density variation due to microbubbles was modeled by introducing CO_2 gas species and using the species transport model. In the species transport model, the local mass fraction of each species, Y_i, is predicted by solving a convection–diffusion equation for the ith species

$$\frac{\partial}{\partial t}(\rho Y_i)+\nabla\cdot(\rho\vec{v}Y_i)=-\nabla\cdot\vec{J}_i+S_i \tag{10}$$

where $\vec{J}_i$ is the diffusion flux of species i and S_i is the rate of creation from any sources. For turbulent flows such as those considered here, the diffusion flux has the following form:

$$\vec{J}_i=-\left(\rho D_{i,m}+\frac{\mu_t}{Sc_t}\right)\nabla Y_i \tag{11}$$

where Sc_t is the turbulent Schmidt number, μ_t is the turbulent viscosity, and $D_{i,m}$ is the diffusion coefficient for species i in the mixture.

The mixture density was computed using the volume-weighted mixing law:

$$\rho_m=\frac{1}{\sum_i\frac{Y_i}{\rho_i}} \tag{12}$$

The mixture viscosity was computed using the mass-weighted mixing law:

$$\mu_m=\sum_i Y_i\mu_i \tag{13}$$

The CO_2 gas was introduced as species mass source in the first layer of cells along the porous section of the flat plate ("Wall 2" on Fig. 1). Zero-gradient condition for all species was used on the flat plate. This model does not capture the physics of the microbubbles; however, it allows one to ascertain whether the simple mixture density variation effect is the dominant source of microbubble drag reduction. The model was solved using the FLUENT 6 CFD solver.

A 712 mm by 250 mm computational domain (Fig. 1) with 113×65 grid nodes (Fig. 2) was used to solve the model. The dimensions of the domain corresponded to those of Merkle and Deutsch (1992) flat plate experimental configuration and to those of Kunz et al. (2003) CFD model to facilitate comparison of the results. To compute gas inlet volumetric flow rates, the depth of the domain was assumed to be 102 mm.

The height of the computational domain was selected so that it would be at least 20 turbulent boundary layer thicknesses, which, for the present case, was about $\delta=10$ mm. Wall-normal clustering of cells was used to resolve the boundary layer, and axial clustering was used near the ends of flat plate sections (Wall 1, Wall 2, and Wall 3 in Fig. 1). Dimensions of the computational domain and boundary conditions are shown schematically in Fig. 1. Constant velocity boundary condition is used in the domain inlet, symmetry boundary conditions are used in the leading part of the domain as well as in the far field above the flat plate to simulate experimental water tunnel conditions, no slip boundary condition is applied at the flat plate, and constant pressure boundary condition is applied at the domain outlet. Values of k and ω at the domain inlet were specified as $1.2\times10^{-5}\ \text{m}^2/\text{s}^2$ and $1.2\times10^{-3}\ \text{s}^{-1}$, respectively. The same values were used as initial guesses for k and ω. These values were selected to facilitate comparison with the CFD results of Kunz et al. (2003) obtained with the same k and ω at the domain inlet.

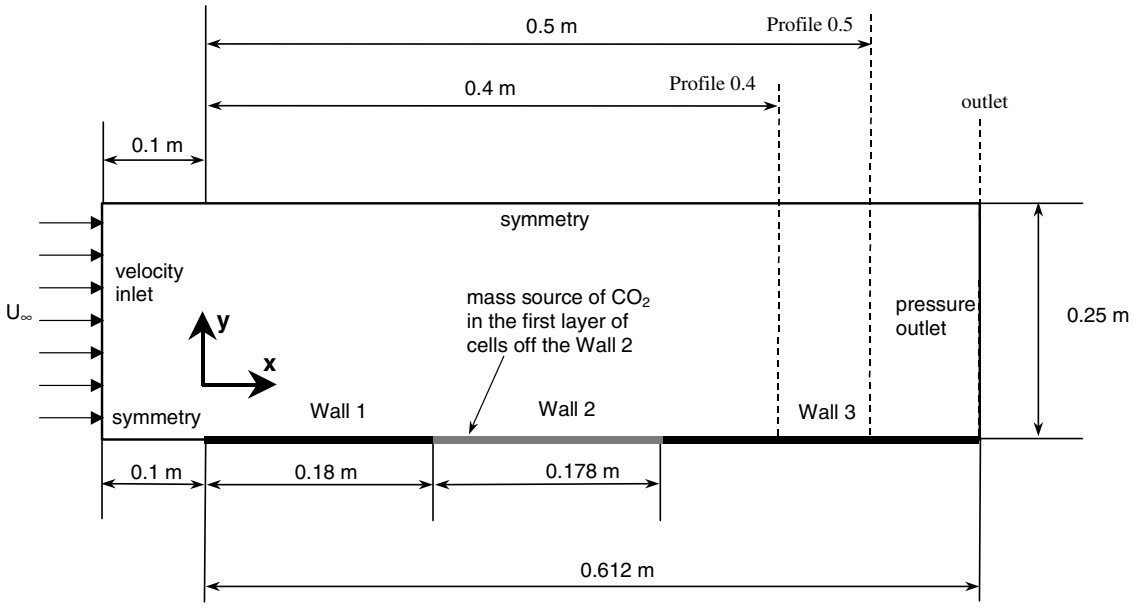

Fig. 1. Schematic diagram of the computational domain.

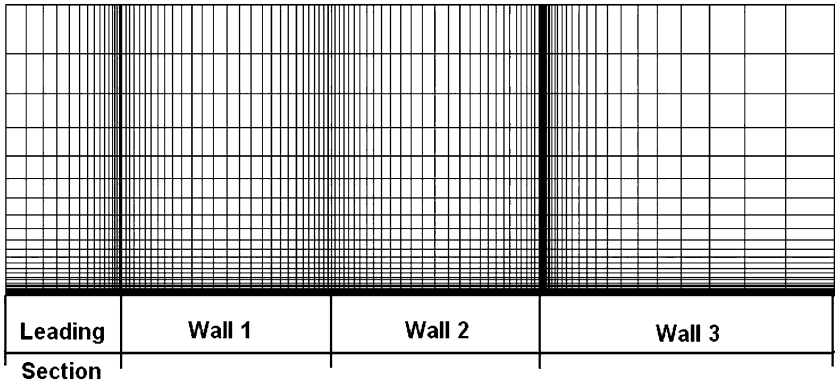

Fig. 2. The 113×65 computational grid.

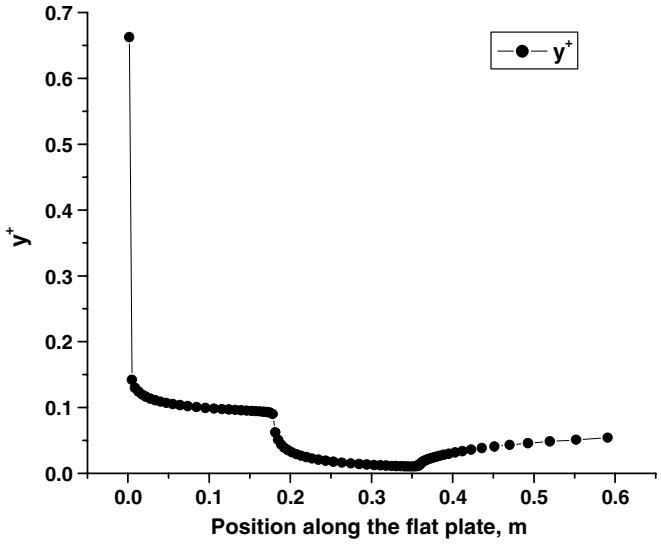

Fig. 3. The y^+ in the first cell of the wall along the flat plate (Wall 1 + Wall 2 + Wall 3) for case of Q3 and $U_\infty = 10.9$ m/s.

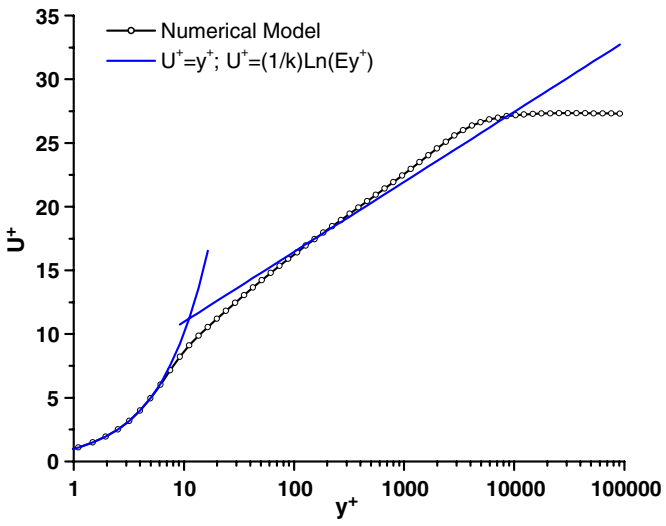

Fig. 4. Comparison of simulated boundary layer velocity profile with standard law of the wall curves.

To validate that the computational grid satisfied $y^+ \leqslant 1$ at the first cell of the wall, the y^+ at the first cell was plotted along the flat plate for all computational cases. A sample plot for the "Q3–V10" case with free stream velocity of 10.9 m/s is shown in Fig. 3. The y^+ values along the flat plate for other studied cases had similar values and are not presented here.

In order to validate the model further, simulated boundary layer velocity profile for the case without gas injection was compared to standard law-of-the-wall curves. Boundary layer velocity profile in the outlet boundary of the computational domain is plotted in Fig. 4 in inner variables and compared to the standard curves. It is seen from the figure that the simulated profile is in good agreement with standard curves.

3. Results and discussion

The ability of our model to predict the drag reduction is validated by comparing our model predictions with the experimental data of Merkle and Deutsch (1992) and with the ensemble averaged multifield two-fluid modeling results of Kunz et al. (2003). Fig. 5 compares computed drag reduction (integrated drag coefficient over "Wall 3" flat plate section normalized by its single-phase value) for a number of nondimensional gas injection flow rates and several free stream velocities. The input conditions for these cases are summarized in Table 1. The figure shows that not only the results of the current model are close to those of the more advanced model of Kunz et al. but also that the current model correctly predicts smaller drag reduction for lower free stream velocity as observed in the experiments. The results of our model are very close to those of Kunz et al. model, however, both models over predict experimentally observed drag reduction by as much as 50% in some cases.

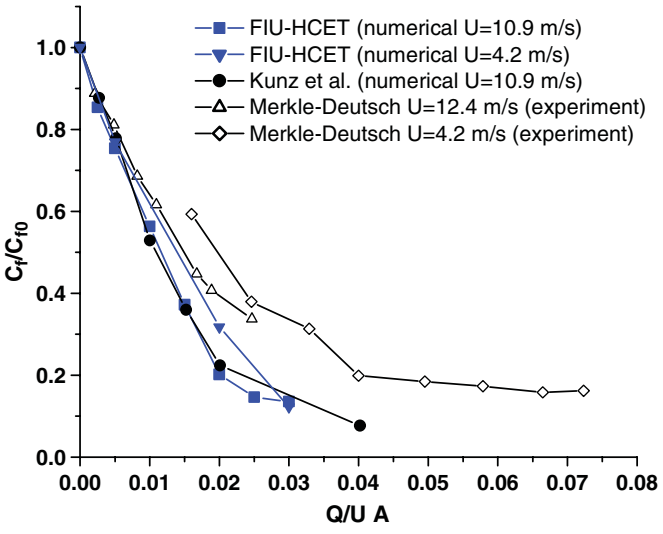

Fig. 5. Comparison of the computed plate drag coefficient with the experimental data of Merkle and Deutsch (1992) and the numerical model of Kunz et al. (2003).

Table 1
Input conditions of computational cases

Case	CO_2 volume flow rate, m^3/s	Nondimensional flow rate, $Q/U_\infty A$	Free stream velocity, m/s	Re_L based on the total plate length
Q0–V10	0	0	10.9	6.67×10^6
Q1–V10	0.0005	0.0025	10.9	6.67×10^6
Q2–V10	0.001	0.005	10.9	6.67×10^6
Q3–V10	0.002	0.01	10.9	6.67×10^6
Q4–V10	0.003	0.015	10.9	6.67×10^6
Q5–V10	0.004	0.02	10.9	6.67×10^6
Q6–V10	0.005	0.025	10.9	6.67×10^6
Q7–V10	0.006	0.03	10.9	6.67×10^6
Q0–V4	0	0	4.2	2.57×10^6
Q1–V4	0.0002	0.0025	4.2	2.57×10^6
Q2–V4	0.0004	0.005	4.2	2.57×10^6
Q5–V4	0.0015	0.02	4.2	2.57×10^6
Q7–V4	0.0023	0.03	4.2	2.57×10^6

A parametric study of the density ratio effect on the drag reduction was carried out. Density ratio is defined as the ratio of the density of the injected gas to that of water. To perform this study, the density of CO_2 gas was varied in the range from 1 to 200 kg/m^3; viscosity of CO_2 was not changed. Table 2 summarizes studied input parameter values.

In order to investigate the effect of density ratio on microbubble drag reduction, one has to ensure that the volumetric concentrations of injected gas are identical for different density ratio values. Fig. 6 shows volumetric concentration profiles for different density ratios at two vertical profiles above the flat plate. These profiles are designated as "outlet" and "profile 0.4" as shown in Fig. 1. The free stream velocity and the nondimensional gas flow rate for all the cases shown in Fig. 6 were the same and equal to 10.9 m/s and 0.005, respectively.

With the exception of the DR = 1 profile, the volumetric concentrations of the injected gas are very similar. The DR = 1 profile corresponds to the case where density of the injected gas is equal to that of water, the results of this simulation are only used to normalize integrated drag coefficient for the other density ratios in order to account for the effect of injection. To quantify the difference between the concentration profiles, they were plotted versus the

Table 2
Input parameters for density ratio effect studies

Density ratio	Gas flow rate, $Q/U_\infty A$	Free stream velocity, m/s
0.001	0.005	10.9
0.001788	0.01	
0.003	0.015	
0.004	0.02	
0.008		
0.02		
0.0333		
0.1		
0.2		

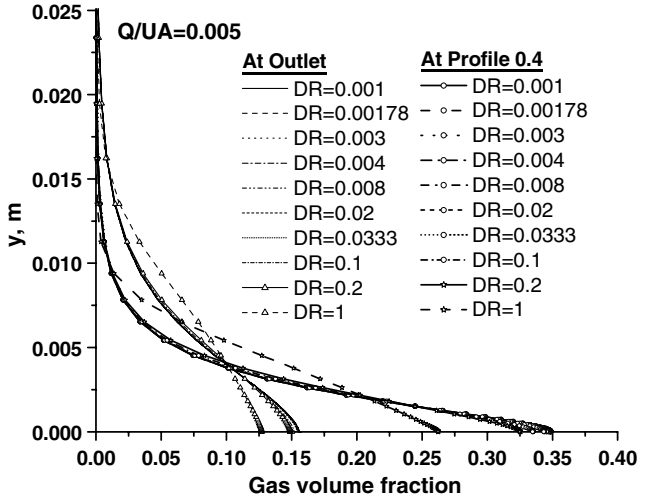

Fig. 6. Computed gas volume fraction profiles in the boundary layer at two vertical profiles above the flat plate ($U = 10.9$ m/s, $Q/U_\infty A = 0.005$).

average concentration profile along with ±5% deviations from it as shown in Figs. 7 and 8. It is seen from Figs. 7 and 8 that all the profiles at the "Outlet" and "Profile 0.4" positions are within 5% of the average profile. This indicates that presented simulation cases can be used to investigate the effect of density ratio on the microbubble drag reduction.

In a similar fashion, Figs. 9–11 show gas volumetric concentration profiles for different density ratios at "Outlet" and "Profile 0.4" positions for the cases with free stream velocity of 10.9 m/s and nondimensional gas flow rates of 0.01, 0.015, and 0.02 respectively. These figures confirm that the differences between gas volumetric concentration profiles for different density ratios are small (except for DR = 1), and thus the simulation cases can be used for the density ratio effect study.

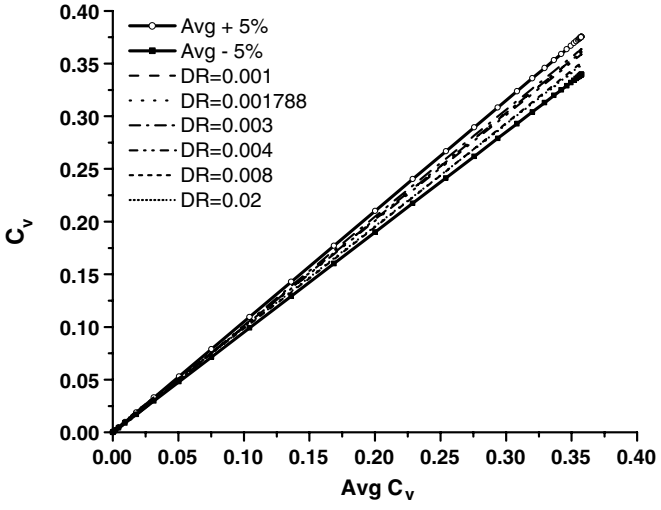

Fig. 7. Comparison of gas volume concentration profiles at "Profile 0.4" above the flat plate ($U = 10.9$ m/s, $Q/U_\infty A = 0.005$).

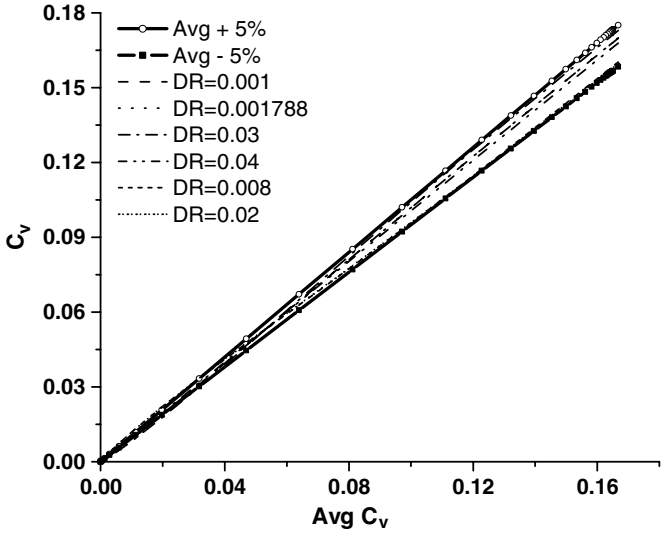

Fig. 8. Comparison of gas volume concentration profiles at "Outlet" above the flat plate ($U = 10.9$ m/s, $Q/U_\infty A = 0.005$).

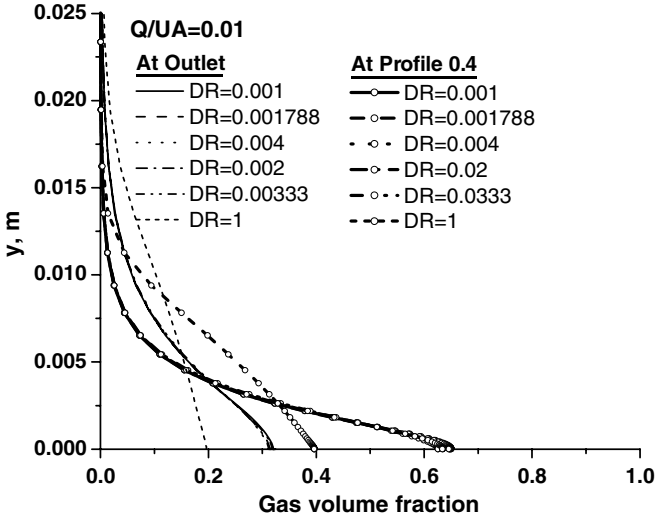

Fig. 9. Computed gas volume fraction profiles in the boundary layer at two vertical profiles above the flat plate ($U = 10.9$ m/s, $Q/U_\infty A = 0.01$).

Effect of density ratio on velocity profiles in the outlet of the computational domain is shown in Fig. 12a and b for cases with different nondimensional gas flow rates. As seen from Fig. 12, the higher the gas flow rate the stronger the effect of density ratio on the velocity profile. For all gas injection rates studied, lower density ratio results in higher velocity gradient in the boundary layer near the flat plate. Away from the boundary layer all velocity profiles become almost identical (this is not shown in Fig. 12).

Changes in turbulent kinetic energy and its production due to the change in density ratio are shown in Figs. 13 and 14. Fig. 13 shows that turbulent kinetic energy production is decreasing with decreasing density ratio and its peak is shifted away from the flat plate. From Fig. 14 it is seen that, while the peak in turbulent kinetic energy is

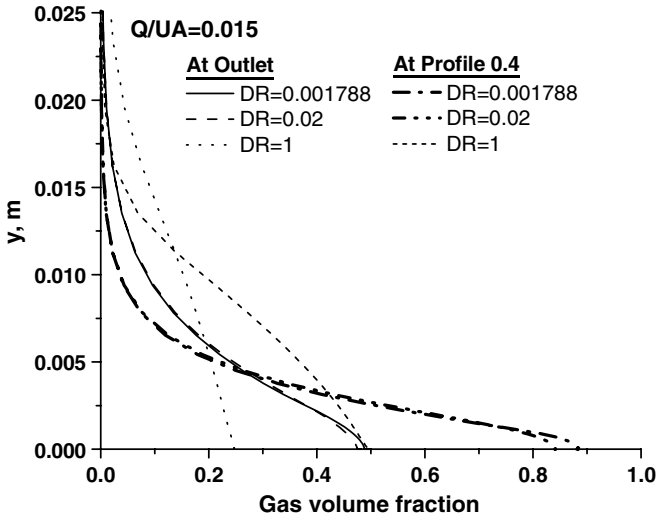

Fig. 10. Computed gas volume fraction profiles in the boundary layer at two vertical profiles above the flat plate ($U = 10.9$ m/s, $Q/U_\infty A = 0.015$).

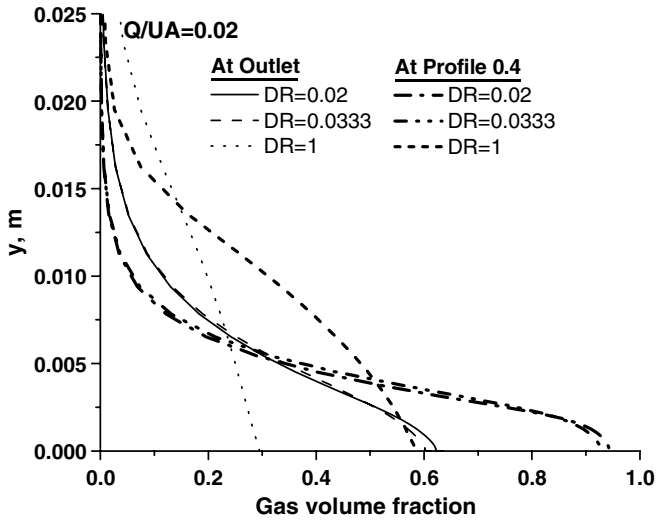

Fig. 11. Computed gas volume fraction profiles in the boundary layer at two vertical profiles above the flat plate ($U = 10.9$ m/s, $Q/U_\infty A = 0.02$).

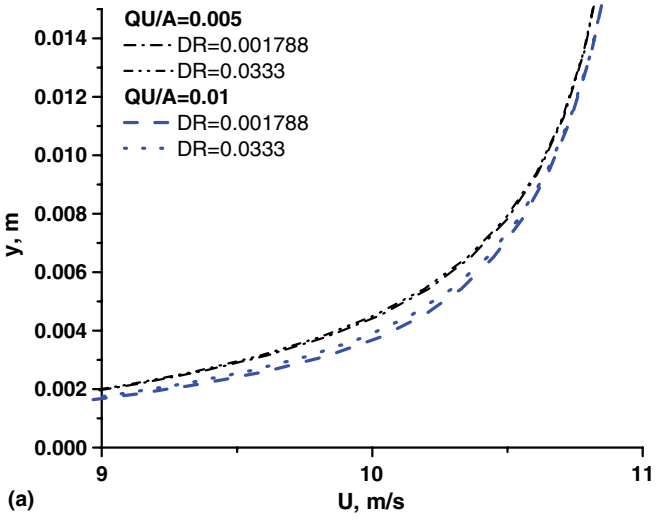

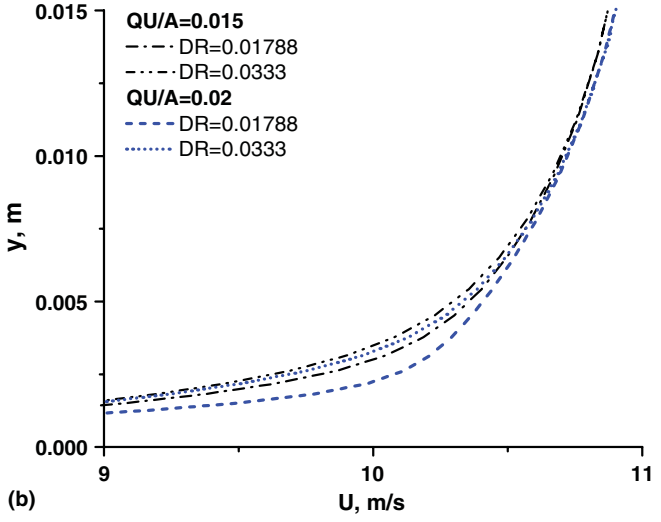

Fig. 12. (a) Computed velocity profiles in the boundary layer at "Outlet" vertical profile above the flat plate ($Q/U_\infty A = 0.005$ and 0.01). (b) Computed velocity profiles in the boundary layer at "Outlet" vertical profile above the flat plate ($Q/U_\infty A = 0.015$ and 0.02).

decreasing with decreasing density ratio, it is also shifted away form the flat plate. This shifting of both turbulent kinetic energy and its production away from the flat plate could be a mechanism responsible for drag reduction.

Effect of density ratio on the drag reduction is shown in Fig. 15, where C_f/C_{f0} ratio is plotted versus the density ratio (ρ_{gas}/ρ_{water}). In this ratio, C_f is the integrated drag coefficient over "Wall 3" flat plate section, and C_{f0} is the integrated drag coefficient over the same flat plate section for DR = 1 ($\rho_{gas} = \rho_{water}$). From Fig. 15 it is seen that for lower gas injection rates ($Q/U_\infty A = 0.005$ and 0.01) with decreasing density ratio, drag reduction quickly assumes the value close to that for CO_2 injection and remains almost unchanging for density ratios between 0.001 and 0.2. The drag reduction for DR = 0.2 is only about 1.7% lower than that for DR = 0.001 for $Q/U_\infty A = 0.005$. For higher gas injection flow rates ($Q/U_\infty A = 0.015$, and 0.02), a gradual increase of the drag reduction with decreasing density ratio is observed. Gradual and substantial increase of the drag reduction up to the lowest density ratio studied indicates that simple mixture density variation effect plays one of the major roles in the microbubble drag reduction phenomenon. The drag reduction is substantially lower for high density ratio values which correspond to high mixture densities resulting from increasing injected gas density. On the other hand, when the density of the injected gas is close to that of CO_2 the drag reduction on the order of that observed experimentally is obtained. Thus, by varying the mixture density alone one can change the drag reduction from none to the maximum value, which shows the important role played by the mixture density in microbubble drag reduction. These results are in qualitative agreement with exper-

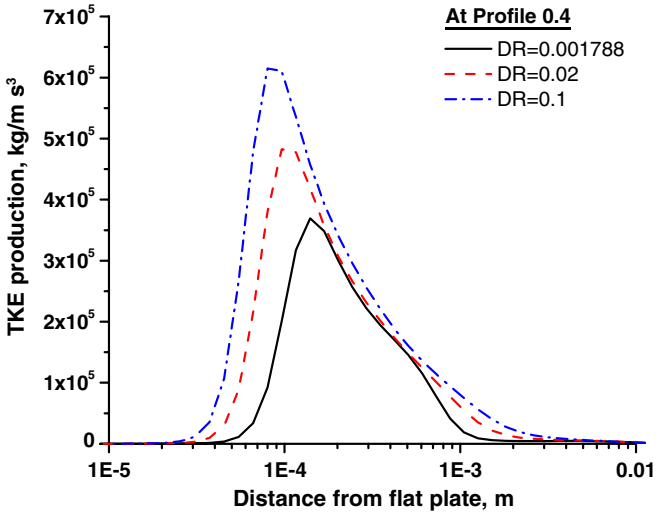

Fig. 13. Turbulent kinetic energy production in the boundary layer at "Profile 0.4" vertical profile above the flat plate ($Q/U_\infty A = 0.015$).

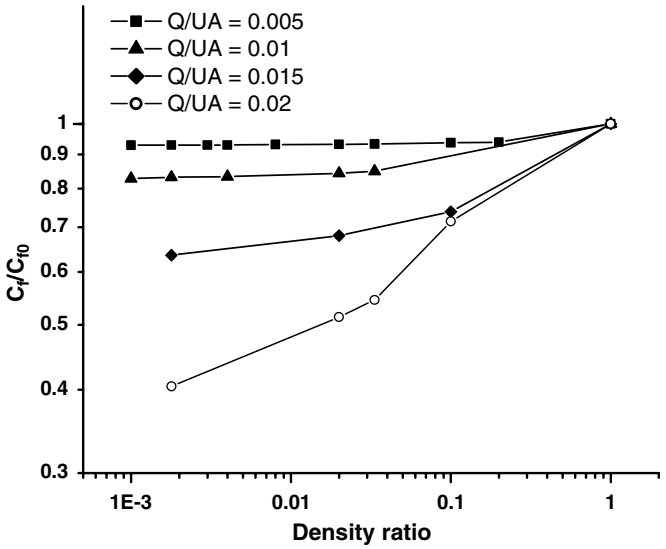

Fig. 15. Density ratio effect on the drag reduction ($U = 10.9$ m/s, $Q/U_\infty A = 0.005$; 0.01; 0.015, and 0.02).

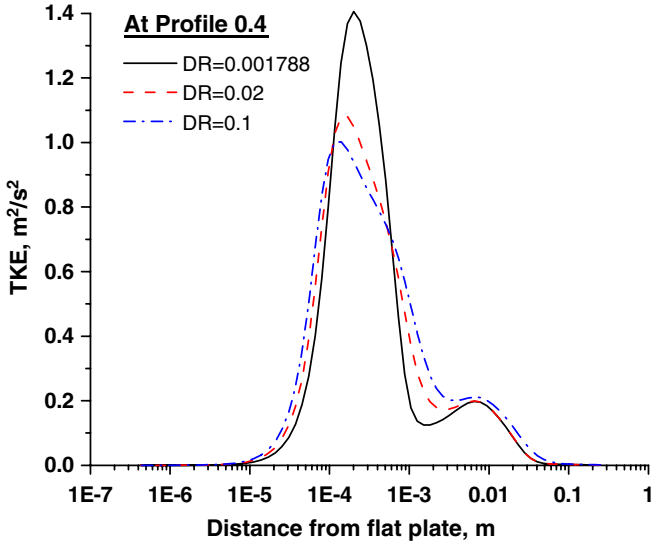

Fig. 14. Turbulent kinetic energy in the boundary layer at "Profile 0.4" vertical profile above the flat plate ($Q/U_\infty A = 0.015$).

imental findings of Pal (1989) and Fontaine and Deutsch (1992). These researches studied the effect of different injection gases on drag reduction. Several gases were studied with densities ranging from 0.1625 kg/m^3 (helium) to 6.17 kg/m^3 (sulfur hexafluoride). It was found that all studied gases were effective in reducing drag. Helium, lowest density gas among the studied gases, was found to be slightly more effective than other gases especially at high gas injection flow rates. Sulfur hexafluoride, highest density gas among the studied gases, was found to be clearly less effective at the higher gas injection rates. Even though the range of density ratios used in the experiments is substantially narrower than that used in our parametric study, these experimental findings confirm our numerical data showing that density ratio (or gas density) effect is more pronounced for high gas injection rates and that smaller density ratios result in higher drag reduction.

4. Conclusions

The single-phase model with bubbles introduced as species mass source was able to predict drag reduction consistent with the experimental data and more complex two-fluid model results.

For low gas injection flow rates: (a) Drag reduction was predicted even for the high density ratio of 0.2 and (b) drag reduction remained almost unchanging for density ratios between 0.2 and 0.001.

For high gas injection flow rates, gradual increase of drag reduction (decrease of the drag coefficient) with decreasing density ratio was predicted, which indicates that simple mixture density variation effect plays one of the major roles in the microbubble drag reduction phenomenon.

These results of our parametric study are in quantitative agreement with the experimental data available for limited range of density ratios.

With decreasing density ratio both turbulent kinetic energy and its production are shifting away from the flat plate, which could be a mechanism responsible for the drag reduction.

Acknowledgements

This work was supported by The Applied Research Laboratory at The Pennsylvania State University, with Dr. Robert F. Kunz as technical monitor. The authors are also thankful to Mr. Manish Mantravadi for his help in running some of the simulation cases used in this paper.

References

Ferrante, A., Elghobashi, S., 2004. On the physical mechanisms of drag reduction in a spatially developing turbulent boundary layer laden with microbubbles. Journal of Fluid Mechanics 503, 345–355.

Fontaine, A.A., Deutsch, S., 1992. The influence of the type of gas on the reduction of skin friction drag by microbubble injection. Experiments in Fluids 13 (2–3), 128–136.

Kanai, A., Miyata, H., 2001. Direct numerical simulation of wall turbulent flows with microbubbles. International Journal for Numerical Methods in Fluids 35 (5), 593–615.

Kawamura, T., Kodama, Y., 2002. Numerical simulation method to resolve interactions between bubbles and turbulence. International Journal of Heat and Fluid Flow 23 (5), 627–638.

Kim, S.-Y., Cleaver, J.W., 1995. The persistence of drug reduction following the injection of microbubbles into a turbulent boundary layer. International Communications in Heat and Mass Transfer 22 (3), 353–357.

Kunz, R.F., Deutsch, S., Lindau, J.W., 2003. Two fluid modeling of microbubble turbulent drag reduction. In: 4th ASME–JSME Joint Fluids Engineering Conference, Honolulu, Hawaii, July 6–11, 2003, Paper FED2003-45640.

Legner, H.H., 1984. A simple model for gas bubble drag reduction. Physics of Fluids 27 (12), 2788–2790.

Madavan, N.K., Merkle, C.L., Deutsch, S., 1985. Numerical investigations into the mechanisms of microbubble drag reduction. Journal of Fluids Engineering 107, 370–377.

Marie, J.L., 1987. Simple analytical formulation for microbubble drag reduction. PhysicoChemical Hydrodynamics 8 (2), 213–220.

McCormick, M.E., Bhattacharya, R., 1973. Drag reduction of a submersible hull by electrolysis. Naval Engineering Journal 85, 11–16.

Meng, J.C.S., Uhlman Jr., J.S., 1998. Microbubble formation and splitting in a turbulent boundary layer for turbulence reduction. In: Proceedings of the International Symposium on Seawater Drag Reduction, 22–23 July 1998, 341–355.

Merkle, C.L., Deutsch, S., 1992. Microbubble drag reduction in liquid turbulent boundary layers. Applied Mechanics Reviews 45 (3), 103–127.

Pal, S., 1989. Turbulence characteristics and bubble dynamics of a microbubble-modified boundary layer. Ph.D. Thesis, Pennsylvania State University.

Wilcox, D.C., 1998. Turbulence Modeling for CFD. DCW Industries, Inc., La Canada, California.

Xu, J., Maxey, M.R., Karniadakis, G.E., 2002. Numerical simulation of turbulent drag reduction using micro-bubbles. Journal of Fluid Mechanics 468, 271–281.